Supporting Information Appendix

SI Materials and Methods

Data collection. As HFRS is a severe viral disease in China, strict criteria were applied in both the clinical diagnosis and reporting (1). Since 1950, HFRS has been listed as a notifiable disease, and all cases are required by law to be reported to the China Center for Disease Control and Prevention. Before the 1980s, HFRS cases were defined by a national standard of clinical criteria in our study area; since the 1980s, cases were also confirmed by detecting antibodies against hantavirus in patients' serum samples (2, 3).

A clinical confirmed case of HFRS was defined as a person who had 1) traveled to the HFRS endemic area or who had come into contact with rodent feces, saliva, and/or urine within 2 months before the onset of illness, 2) who had an acute illness characterized by abrupt onset and presented the following clinical features: fever, chills, hemorrhage, headache, back pain, abdominal pain, acute renal dysfunction, hypotension, and 3) must exhibit five distinct disease phases: the pyretogenesis phase, shock phase, oliguria phase, diuretic phase, and recovery phase.

We also conducted the analysis using the dataset from 1980–2013. The results consistently supported our previous analysis (Fig. 1*C*), and the time series of HFRS incidence and rodent population density showed interannual oscillations of 8–10 years (*SI Appendix*, Fig. S7).

Wavelet coherence. The wavelet coherence is a useful tool to analyze patterns of co-variation between two time series (4) and has been used to quantify the non-stationary relationship between HFRS time series, capture rate, and climate variables:

$$S_x(f,t) = \left\| W_x(f,t) \right\|^2 \qquad [1]$$

$$C_{xy}(f,t) = \left(\frac{\left\| \left\langle W_{xy}(f,t) \right\rangle \right\|}{\left\| \left\langle W_x(f,t) \right\rangle \right\|^2 \cdot \left\| \left\langle W_y(f,t) \right\rangle \right\|^2} \right)^{1/2} \qquad [2]$$

where $W_{xy}(f,t) = W(f,t) \cdot W_x^*(f,t)$ is the wavelet cross-spectrum, * denoting the complex conjugate.

To account for the interactions between local and global climatic variables on the HFRS dynamics, the partial wavelet coherence was used. The partial wavelet coherence, a technique similar to partial correlation, can identify the resulting wavelet coherence between two time series after eliminating the influence of a third common dependence (5). The partial wavelet coherence between *x*(*t*) and *y*(*t*) corrected by the coherence of *z*(*t*) reads:

$$PC_{xy|z}(f,t) = \frac{\left\| C_{xy}(f,t) - C_{xz}(f,t) \cdot C_{yz}^*(f,t) \right\|^2}{\left\| 1 - C_{xz}(f,t) \right\|^2 \cdot \left\| 1 - C_{yz}(f,t) \right\|^2} \qquad [3]$$

Analyses were performed using Matlab (version 6.5; MathWorks Inc., Natick, MA, USA).

SI References

1. Zhang YZ, Zou Y, Fu ZF, & Plyusnin A (2010) Hantavirus infections in humans and animals, China. *Emerg Infect Dis* 16(8):1195-1203.
2. Yu P, *et al.* (2015) Hantavirus infection in rodents and haemorrhagic fever with renal syndrome in Shaanxi province, China, 1984–2012. *Epidemiol Infect* 143(2):405-411.
3. Tian H, *et al.* (2017) Anthropogenically driven environmental changes shift the ecological dynamics of hemorrhagic fever with renal syndrome. *PLoS Pathog* 13(1):e1006198.
4. Cazelles B, Chavez M, de Magny GC, Guégan J-F, & Hales S (2007) Time-dependent spectral analysis of epidemiological time-series with wavelets. *J R Soc Interface* 4(15):625-636.
5. Ng EK & Chan JC (2012) Geophysical applications of partial wavelet coherence and multiple wavelet coherence. *J Atmos Ocean Technol* 29(12):1845-1853.

SI Figures

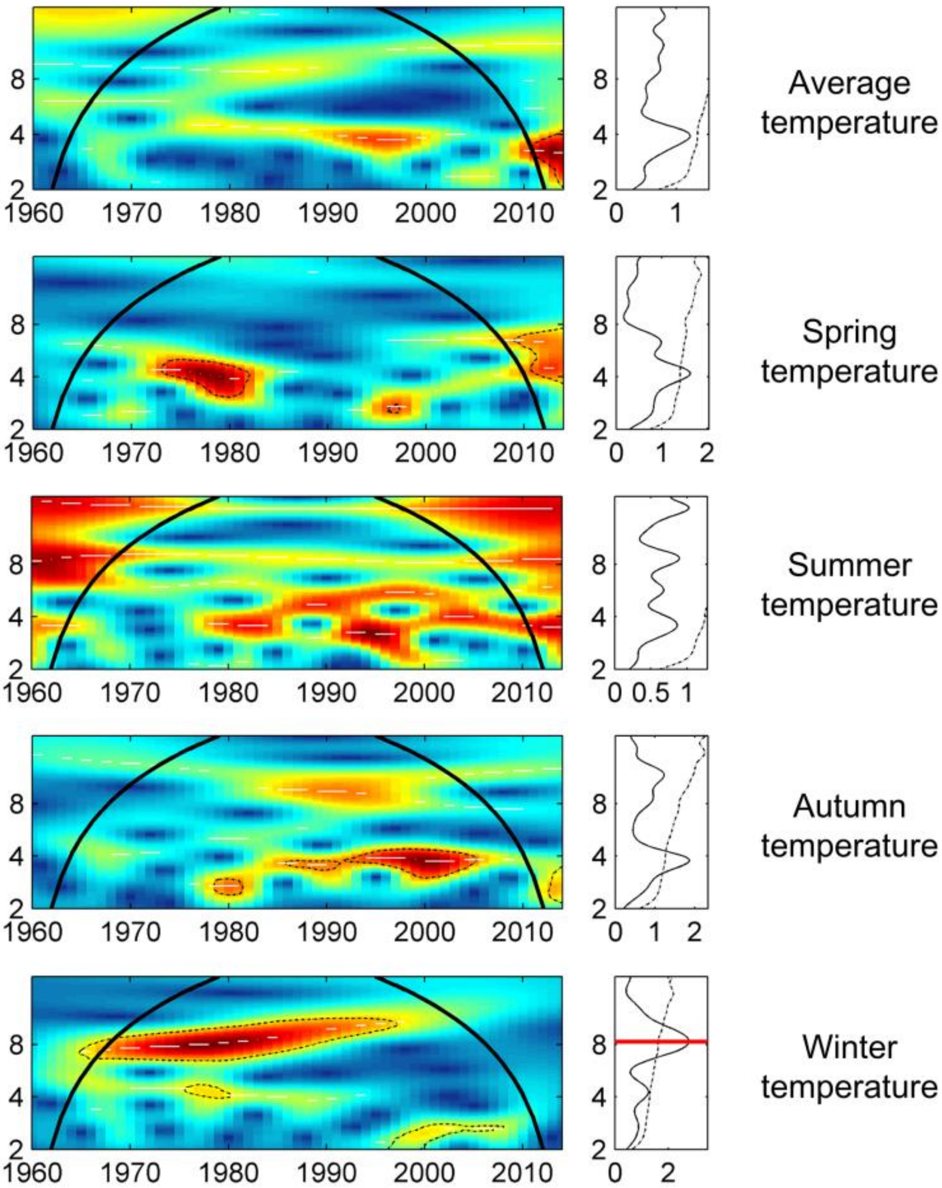

Fig. S1 Wavelet power spectra showing the periodicity of the average temperature, spring temperature, summer temperature, autumn temperature and winter temperature.

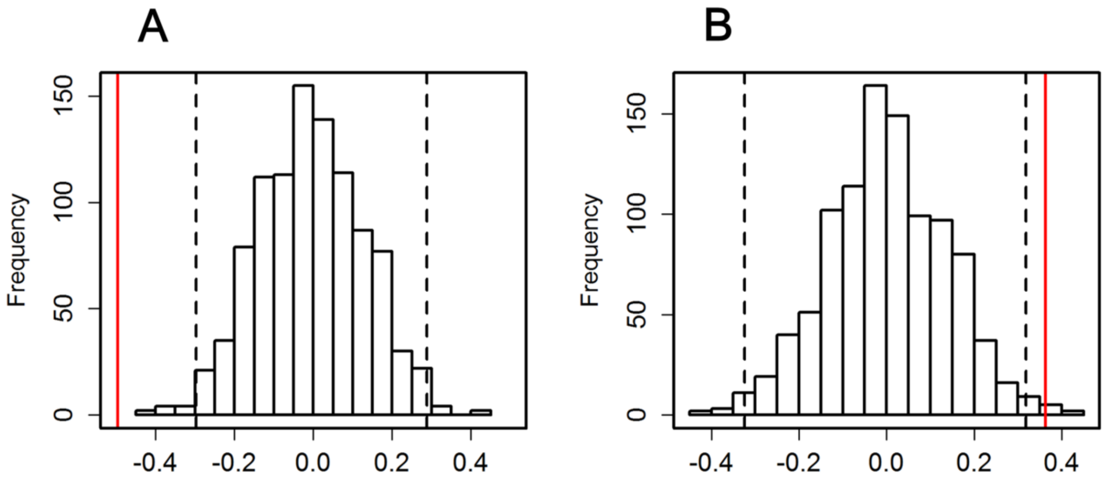

Fig. S2 (*A*) Randomization tests of the correlation between the summer temperature and the incidence of HFRS. (*B*) Randomization tests of the correlation between the summer rainfall and the incidence of HFRS. The red line shows the observed correlation, and the dashed lines the 95 percentiles for the correlations expected from random permutations of the series.

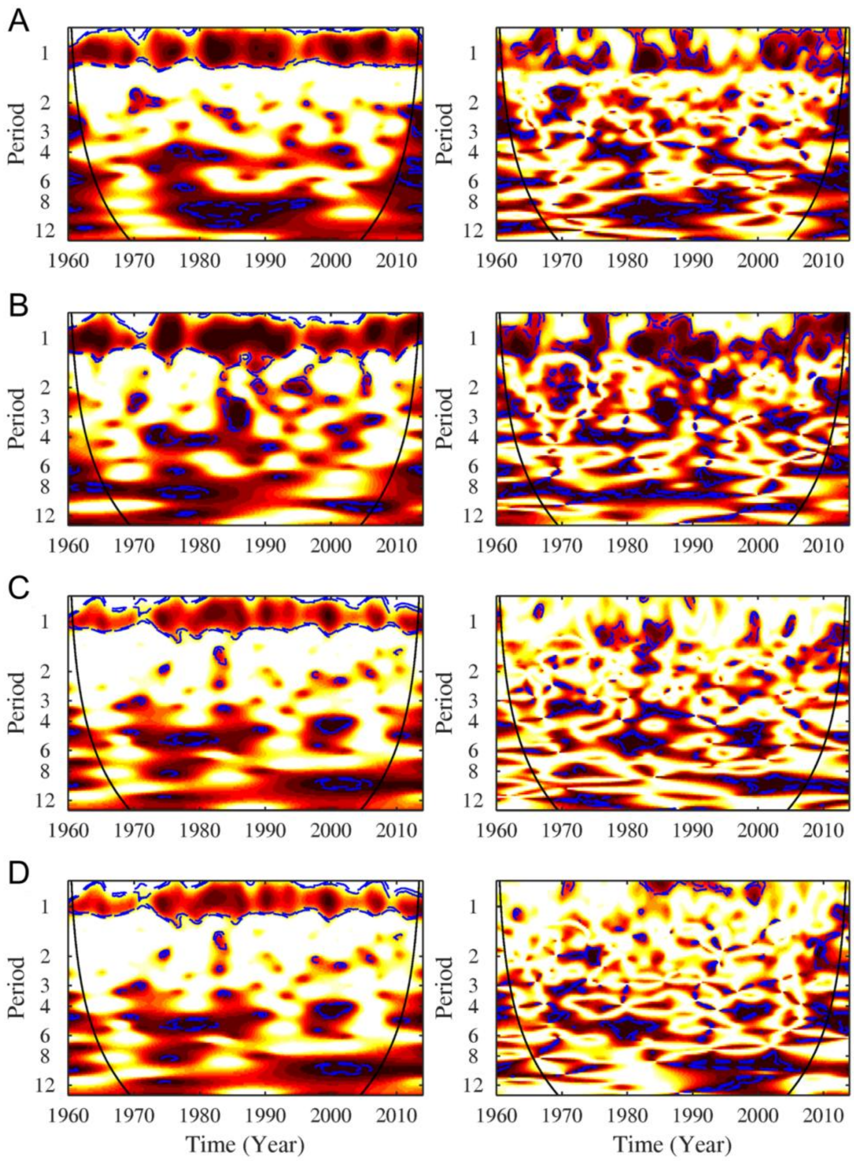

Fig. S3 Wavelet coherence and partial wavelet coherency between HFRS and local and global climate. Left panel: Wavelet Coherence; Right panel: Partial Wavelet Coherence. (*A*) HFRS and temperature time series coherence (left panel) corrected by the Nino3.4 index (right panel). (*B*) HFRS and rainfall time series coherence (left panel) corrected by the Nino3.4 index (right panel). (*C*) HFRS and the Nino3.4 index coherence (left panel) corrected by temperature time series (right panel). (*D*) HFRS and the Nino3.4 index coherence (left panel) corrected by rainfall time series (right panel). In the wavelet power spectra, the blue dotted lines correspond to the 5% and 10% significance levels, and the bold line is known as the cone of influence. The cone of influence delimits the effect of the treatment of the boundaries, and the power values are color coded from white (low values) to dark red (high values). Our results clearly show that ENSO cannot explain the seasonal coherence between HFRS epidemics and climatic variables, further emphasizing that local climate is responsible for this statistically significant association. Indeed, this significant association for the seasonal mode does not disappear when local climate coherence is corrected for the ENSO index (*SI Appendix*, Fig. S4 A-B, right panel). Instead, when corrected by local climate (temperature or rainfall), the significant coherence between HFRS epidemics and ENSO vanishes (*SI Appendix*, Fig. S4 C-D, right panel). For multiannual components (mainly following a 8-10 year cycle) the situation appears more complex, as a significant relationship for these components persists more or less in the partial wavelet coherency (*SI Appendix*, Fig. S4). This demonstrates that both local and global climate conditions influence the multiannual associations with HFRS epidemics, and indicates that the dynamical effects of wildlife propagation are dependent on climate-linked multiannual processes.

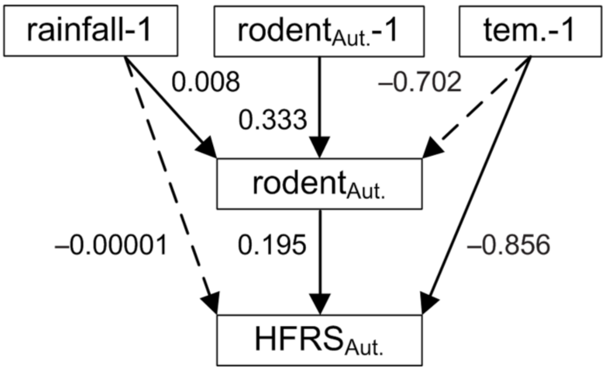

Fig. S4 Structure and results from our structural equation models for climate-linked peak season of HFRS epidemics. Values associated with arrows represent standardized path coefficients. The dashed lines represent nonsignificant paths; -1, previous year; rainfall, total annual rainfall; tem., mean annual temperature; rodent$_{Aut.}$, capture rate of *A. agrarius* in autumn; HFRS$_{Aut}$, incidence of HFRS in autumn. Rainfall has an indirect positive effect via rodents on HFRS epidemics ($P < 0.05$).

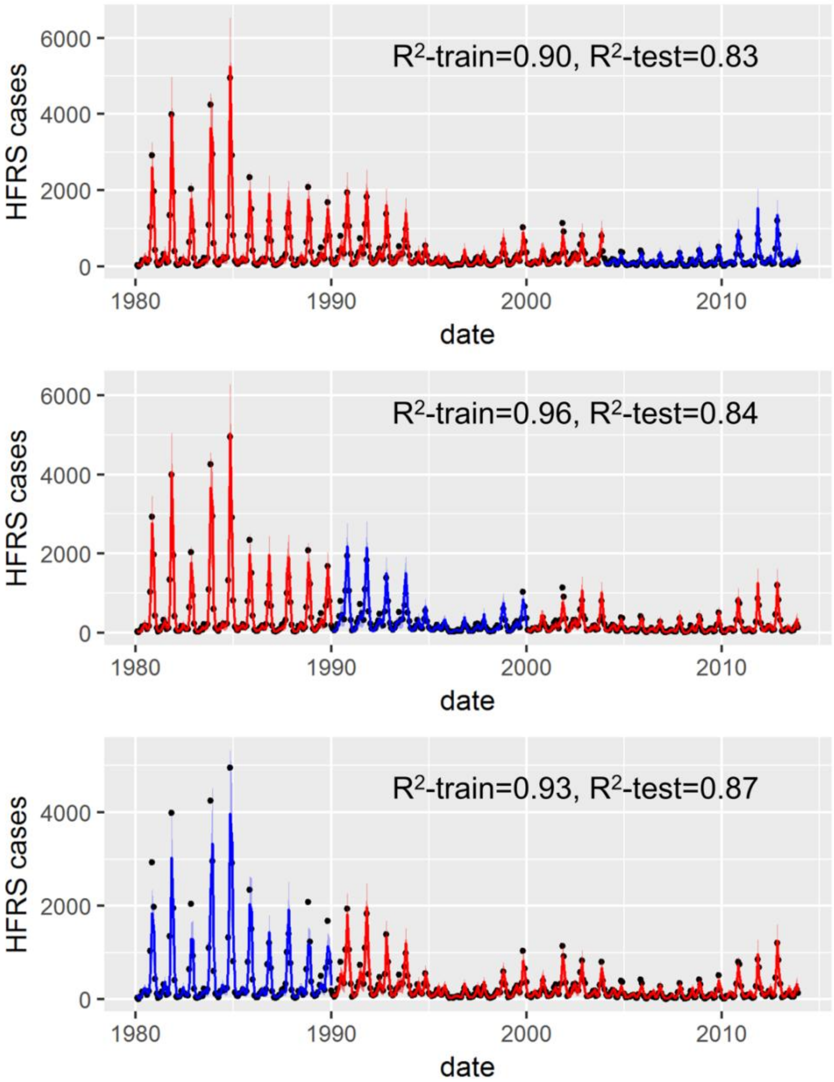

Fig. S5 Cross-validation. Observations are in black, fitted values are in red and predictions are in blue. The average R^2-train and R^2-test of cross validation are 0.93 and 0.85, respectively. Upper panel: models trained on 1980–2003 data, and predictions for 2004–2013; middle panel: models trained on 1980–1989 and 2000–2013 data, and predictions for 1990–1999; lower panel: models trained on 1990–2013 data, and predictions for 1980–1989.

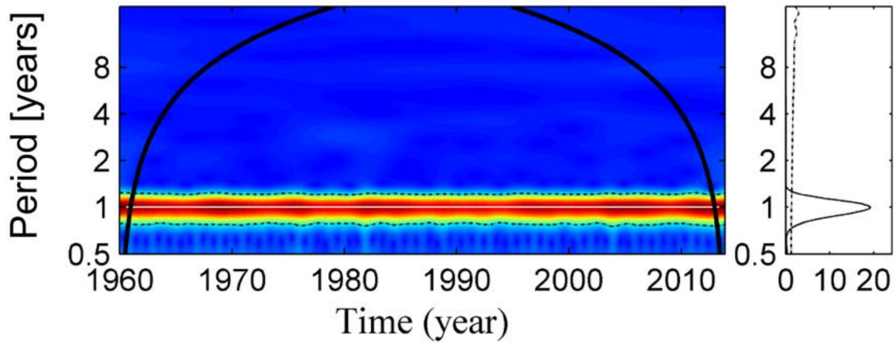

Fig. S6 Wavelet power spectra showing the periodicity of the estimated transmission rate. (*Left*) wavelet power spectra and (*right*) global wavelet power spectra. In the wavelet power spectra, the dotted line corresponds to the 5% significance level, and the bold line is known as the cone of influence. The cone of influence delimits the effect of the treatment of the boundaries, the white lines materialize the maxima of the undulations of the wavelet power spectra, and the power values are color coded from blue (low values) to red (high values). The right panels show the mean spectrum (solid line) with its significant threshold value of 5% (dashed line).

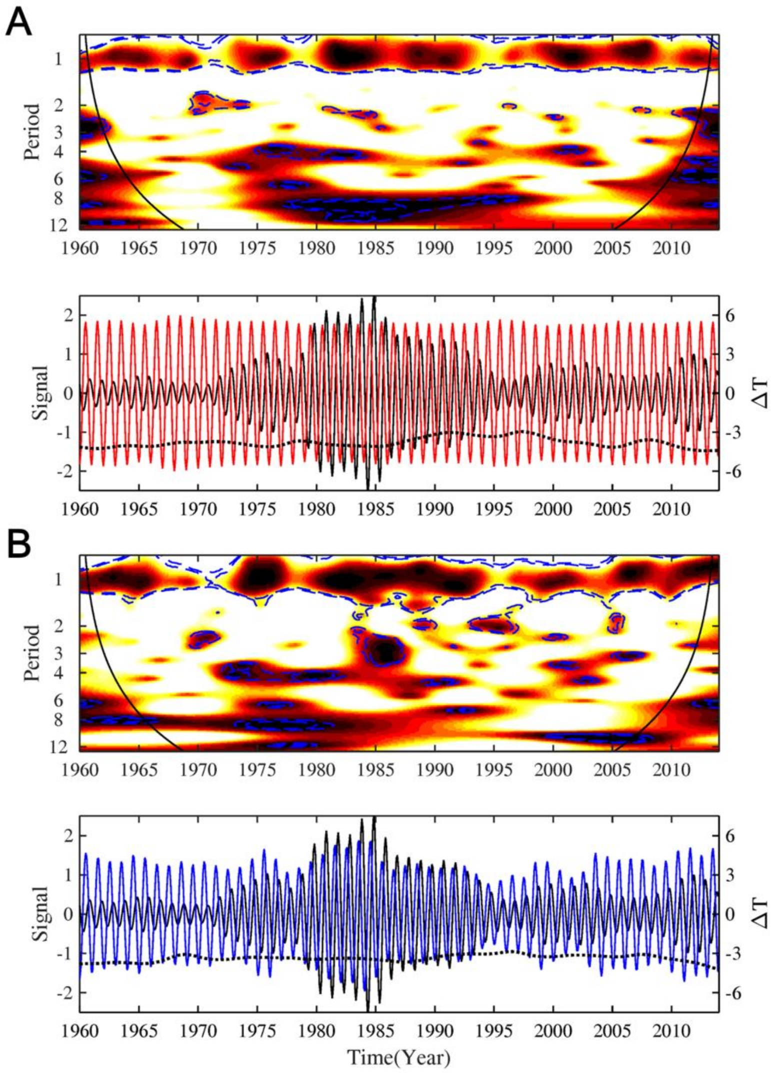

Fig. S7 Association between climatic factors and number of HFRS cases. (*A*) Association between average monthly temperature and hantavirus epidemics, wavelet coherence; the panel below is the annual oscillating component (0.8-1.2 yr) evolutions of the considered series computed with the wavelet transform. (*B*) Association between rainfall and the number of HFRS cases, wavelet coherence; the panel below is the annual oscillating component (0.8-1.2 yr) evolutions of the considered series computed with the wavelet transform. The coherence power spectra (x-axis: time in year; y-axis: period in year), where power is coded from a low value (white) to a high value (dark red). The dotted black lines show the 5% significance level, computed on 1,000 bootstrapped series. The inner area, within the cone of influence (black line), indicates the region not influenced by edge effects. Red line: temperature; blue line: rainfall; black lines: HFRS cases; dotted lines: instantaneous time difference between the oscillating components.

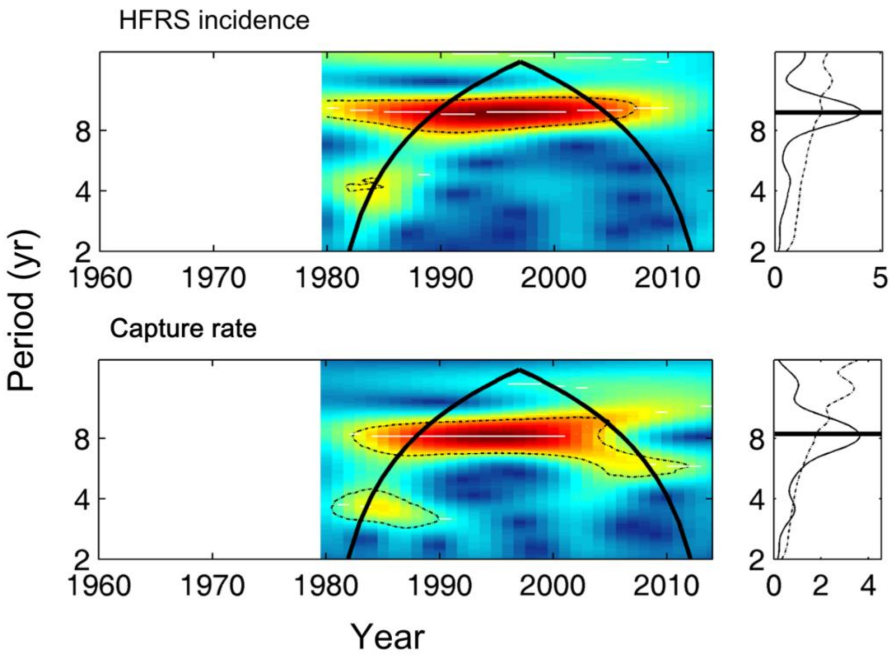

Fig. S8 Wavelet power spectra showing the periodicity of the incidence of HFRS and capture rate of *A. agrarius*, 1980–2013.

Table S1. Yearly and seasonal structural equation models for climate-linked HFRS epidemics in the Weihe Plain.

Climate variables		Standardized path coefficients					Indirect effect				
Rainfall	Temperature	Rodent-1 ↓ Rodent	Temperature ↓ Rodent	Rainfall ↓ Rodent	Rodent ↓ HFRS	Temperature ↓ HFRS	Rainfall ↓ HFRS	Temperature ↓ HFRS	Rainfall ↓ HFRS	χ^2/df	RMSEA	CFI
Spring	Spring	0.48**	-0.18	0.02	0.92**	-0.58**	-0.01	-0.17	0.01	6.66/4	0.14	0.94
Spring	Summer	0.48**	-0.43*	0.02	0.89**	-0.78**	-0.01	-0.39*	0.01	6.69/4	0.14	0.95
Spring	Autumn	0.46**	-0.14	0.02*	0.89**	-0.65**	0.01	-0.12	0.02*	27.72/4	0.42	0.63
Spring	Winter-1	0.48**	-0.13	0.02	1.02**	0.10	-0.01	-0.14	0.02	7.31/4	0.16	0.92
Spring	Yearly-1	0.37**	-0.79**	0.02**	0.77**	-1.14**	0.002	-0.61**	0.02**	9.17/4	0.20	0.91
Summer	Summer	0.53**	-0.44*	0.001	0.85**	-0.77**	0.001	-0.37*	0.001	13.89/4	0.27	0.82
Summer	Spring	0.51**	-0.21	0.01	0.85**	-0.52**	0.01	-0.18	0.01	4.99/4	0.08	0.98
Summer	Autumn	0.59**	0.21	0.01	0.89**	-0.58**	0.01*	0.19	0.01	8.73/74	0.19	0.90
Summer	Winter-1	0.54**	-0.03	0.01	0.95**	0.13	0.01*	-0.03	0.01	6.90/4	0.14	0.92
Summer	Yearly-1	0.46**	-0.57*	0.01	0.77**	-1.05**	0.01	-0.44*	0.004	7.77/4	0.17	0.92
Autumn	Autumn	0.61**	0.32	0.01	0.90**	-0.41*	0.01*	0.28	0.01	14.27/4	0.28	0.81
Autumn	Spring	0.50**	-0.22	0.004	0.84**	-0.50**	0.02**	-0.19	0.003	4.83/4	0.07	0.98
Autumn	Summer	0.53**	-0.47*	-0.001	0.85**	-0.65**	0.01	-0.40*	-0.001	11.15/4	0.23	0.87
Autumn	Winter-1	0.53**	-0.02	0.004	0.95**	0.33	0.02**	-0.02	0.004	11.52/4	0.24	0.85
Autumn	Yearly-1	0.46**	-0.67**	-0.002	0.79**	-0.93**	0.01	-0.53**	-0.002	14.79/4	0.28	0.82
Winter-1	Winter-1	0.54**	-0.09	-0.03	0.98**	0.09	0.04	-0.09	-0.03	5.00/4	0.09	0.97
Winter-1	Spring	0.52**	-0.22	-0.03	0.88**	-0.55**	0.04	-0.20	-0.03	4.03/4	0.02	0.99
Winter-1	Summer	0.53**	-0.44*	-0.02	0.86**	-0.83**	0.05	-0.37*	-0.02	5.11/4	0.09	0.98

Winter-1	Autumn	0.61**	0.22	-0.03	0.92**	-0.58**	0.04	0.20	-0.03	8.60/4	0.19	0.90
Winter-1	Yearly-1	0.47**	-0.62*	-0.03	0.79**	-1.10**	0.03	-0.49*	-0.03	5.70/4	0.11	0.97
Yearly-1	Yearly-1	0.43**	-0.34	0.003**	0.77**	-1.08**	0.001	-0.26	0.002**	13.16/4	0.26	0.85
Yearly-1	Spring	0.42**	-0.26	0.004**	0.76**	-0.58**	0.003*	-0.19	0.003**	6.18/4	0.13	0.96
Yearly-1	Summer	0.46**	-0.28	0.003**	0.82**	-0.76**	0.001	-0.23	0.003**	10.45/4	0.22	0.89
Yearly-1	Autumn	0.58**	0.59**	0.005**	0.90**	-0.54**	0.001	0.53**	0.005**	16.68/4	0.31	0.79
Yearly-1	Winter-1	0.46**	0.04	0.004**	0.89**	0.12	0.002	0.03	0.003**	8.09/4	0.17	0.91

* with significant effect, -1 previous year. Normalized chi-square (model chi-square divided by the degrees of freedom, χ^2/df) was used as a model test statistic, to verify whether the covariance matrix implied by conceptual model is close enough to the sample matrix that the differences may be reasonably considered as due to sampling error. AIC: the Akaike Information Criterion. BIC: the Bayesian information criterion. RMSEA: root mean-square error of approximation. CFI: comparative fit index.

Table S2. Parameter estimates for the selected best model of rodent population

Parameters	Edf*	F	*P*-value
N_{y-1}, rodent density	2.72	4.26	<0.05
T_{y-1}^{winter}, winter temperature	4.49	2.61	<0.10
R_{y-1}, annual rainfall	1.00	8.331	<0.05

Approximate significance of smoothed terms is given as the *P* values.

*Edf is the estimated degree of freedom of the examined covariate. An Edf equal to 1 implies a linear effect and values greater than 1 indicate a progressively stronger nonlinear effect.

Table S3. Posterior estimates, standard deviations (S.D.) for the parameters of the human hantavirus transmission model

Parameters	Estimate	S.D.
δ_1	1.23E-4	8.31E-5
δ_2	5.10E-4	1.01E-4
δ_3	-2.50E-3	2.00E-3
δ_4	-1.13E-2	3.56E-3
α_1	0.75	0.03
α_2	0.06	0.01
ε	0.47	0.11
τ	0.06	0.07
φ_1	4.79	1.18
φ_2	8.14	1.58
φ_3	9.21	1.7
φ_4	14.67	3.39
φ_5	15.02	4.12
φ_6	12.01	3.44
φ_7	9.69	2.06
φ_8	13.8	3.68
φ_9	72.61	16.86
φ_{10}	81.85	18.96
φ_{11}	24.76	6.62
φ_{12}	7.57	1.61